

Evidence for strong electronic correlations in the spectra of Sr_2RuO_4

Z.V. Pchelkina,¹ I.A. Nekrasov,² Th. Pruschke,³ A. Sekiyama,⁴ S. Suga,⁴ V.I. Anisimov,⁵ and D. Vollhardt⁶

¹*Institute of Metal Physics, Russian Academy of Sciences-Ural Division, 62041 Yekaterinburg GSP-170, Russia**

²*Institute of Electrophysics, Russian Academy of Sciences-Ural Division, 620016 Yekaterinburg, Russia*

³*Institute for Theoretical Physics, University of Göttingen, Tammannstr. 1, 37077 Göttingen, Germany*

⁴*Graduate School of Engineering Science, Osaka University Toyonaka, Osaka 560-8531 Japan*

⁵*Institute of Metal Physics, Russian Academy of Sciences-Ural Division, 620219 Yekaterinburg GSP-170, Russia*

⁶*Theoretical Physics III, Center for Electronic Correlations and Magnetism,
University of Augsburg, 86135 Augsburg, Germany*

(Dated: June 23, 2021)

The importance of electronic correlation effects in the layered perovskite Sr_2RuO_4 is evidenced. To this end we use state-of-the-art LDA+DMFT (Local Density Approximation + Dynamical Mean-Field Theory) in the basis of Wannier functions to compute spectral functions and the quasiparticle dispersion of Sr_2RuO_4 . The spectra are found to be in good agreement with various spectroscopic experiments. We also calculate the \mathbf{k} -dependence of the quasiparticle bands and compare the results with new angle resolved photoemission (ARPES) data. Two typical manifestations of strong Coulomb correlations are revealed: (i) the calculated quasiparticle mass enhancement of $m^*/m \approx 2.5$ agrees with various experimental results, and (ii) the satellite structure at about 3 eV binding energy observed in photoemission experiments is shown to be the lower Hubbard band. For these reasons Sr_2RuO_4 is identified as a strongly correlated 4d electron material.

PACS numbers: 71.27.+a, 79.60.-i

I. INTRODUCTION

Intensive research on Sr_2RuO_4 began after the discovery of superconductivity at temperatures below 1 K.¹ Since it is widely believed that this system may help to clarify the mechanism behind high- T_c superconductivity, considerable theoretical and experimental effort was put into the investigation of this material which has unconventional properties in spite of a relatively simple electronic structure. While it is generally recognized that in 3d transition metal compounds electron correlations play a crucial role,² the question whether the 4d system Sr_2RuO_4 should be considered a strongly correlated system, too, or whether its electronic properties can be understood within conventional band theory remained open. Indeed, the 4d states of the Ru-ion are more extended than the 3d states and hence correlation effects should be less significant than, e.g., in high- T_c cuprates. On the other hand, the effective quasiparticle mass obtained from de Haas-van Alphen (dHvA),³ ARPES⁴ and infrared optical experiments⁵ is 3-4 times larger than the results obtained from standard band calculations.^{6,7,8} The temperature-independent contribution to the magnetic susceptibility and specific heat constant¹ are also significantly larger than that given by LDA.⁶ These facts indicate that electron correlations play an important role in Sr_2RuO_4 .

During the last decade intensive studies of Sr_2RuO_4 using various spectroscopic techniques were performed.^{9,10,11,12,13,14,15} The evidence derived from these experiments which point towards correlation effects can be summarized as follows: (i) the measured bandwidth and density of states (DOS) at the Fermi level deviate by roughly a factor of 3^{9,10} from bandstructure calculations,^{6,7,8} and (ii) there is a peculiar satellite at -3 eV in the photoemission spectra (PES).^{12,13,14,15}

The presence of a satellite structure in PES on transition metal oxides, now commonly interpreted as the lower Hubbard band (LHB), is generally taken as strong evidence for the importance of correlations. Such a satellite was first experimentally observed by Fujimori *et al.*¹⁶ for the d^1 perovskite-type Ti^{3+} and V^{4+} oxides. By applying the *ab initio* LDA+DMFT approach^{17,18,19,20,21,22} the corresponding structure in the many-body spectrum was later indeed identified as the LHB.^{17,19,23,24,25} While in d^1 compounds the 3d-band is usually well separated from the oxygen 2p band (making the experimental observation and theoretical interpretation as the LHB relatively simple) the energy separation between the Ru-4d and O-2p states in Sr_2RuO_4 is much smaller (see below). In this case the LHB may overlap with the oxygen 2p bands, making the interpretation of structures in the experimental spectra ambiguous. The difference in experimental conditions (photon energy, surface sensitivity, sample and surface quality, etc) complicate the situation even more. Therefore interpretations of spectroscopic data for Sr_2RuO_4 are often controversial.

Early investigations of the electronic structure of Sr_2RuO_4 used the local density approximation (LDA) to reveal the similarities and differences with the electronic properties of cuprate superconductors.^{6,7} It was then proposed that the superconductivity of Sr_2RuO_4 may be unconventional, namely of triplet type;^{26,27} see the comprehensive reviews.^{28,29} A quantitative model for triplet superconductivity based on first principles calculations for the electronic structure and magnetic susceptibility was suggested by Mazin and Singh.³⁰ The electronic structure of Sr_2RuO_4 and

Sr_2RuO_4 was compared in⁸ and the possibility of a magnetic ground state of Sr_2RuO_4 was studied within the general gradient approximation (GGA).³¹

The Fermi surface of Sr_2RuO_4 was also investigated by LDA. According to these studies, the Fermi surface consists of three cylindrical sheets,^{6,7,8,32} in agreement with dHvA experiments.³ By contrast, ARPES experiments predicted a significantly different Fermi-surface topology.^{33,34,35} In principle, such a discrepancy may be due to strong electronic correlations which are not taken into account in LDA. However, detailed photoemission studies⁴ and scanning-tunneling microscopy³⁶ subsequently discovered a surface reconstruction which seemed to resolve the controversy.^{37,38}

The importance of correlation effects was studied by Pérez-Navarro *et al.*³⁹ and Arita *et al.*⁴⁰ Although correlations are not very strong, their inclusion was found to be important for a proper description of the electronic structure³⁹ and a microscopic understanding of superconductivity.⁴⁰

A first multi-band investigation based on the dynamical mean-field theory (DMFT) to clarify the discrepancy between dHvA³ and photoemission^{34,35} data was performed by Liebsch and Lichtenstein.⁴¹ They observed a charge flow from the narrow xz , yz bands to the wide xy band leading to a shift of the van Hove singularity close to E_F , and derived quasiparticle bands by self-consistent second-order perturbation theory for the self-energy, finding a mass renormalization of 2.1-2.6⁴¹ in agreement with experiment.^{3,4} Anisimov *et al.*⁴² investigated the isoelectric series of alloys $\text{Ca}_{2-x}\text{Sr}_x\text{RuO}_4$ by means of LDA+U for $x = 0$ and DMFT(NCA) for $0.5 < x < 2.0$. In the latter doping range the scenario of an orbital selective Mott transition (OSMT) was proposed.

In this paper we address the question of the importance of correlation effects in Sr_2RuO_4 by a realistic LDA+DMFT(QMC) calculation within a Wannier function (WF) formalism.⁴³ This improved LDA+DMFT(QMC) scheme allows one to take into account the influence of correlated orbitals ($4d$ - t_{2g} orbitals of Ru in our case) on all other states. This is essential when d and oxygen p states overlap as is the case in Sr_2RuO_4 . The comparison between our theoretical results and experiment clearly shows that electronic correlations have a strong influence on the electronic structure and lead to the formation of a pronounced LHB in the spectrum.

The paper is organized as follows. In section II we present results for the band structure obtained by LDA (subsection II.A) and LDA+DMFT(QMC) in the WF basis (subsection II.B), respectively. Section III contains a comparison of our LDA+DMFT(QMC) results with XPS (x-ray photoemission spectroscopy), XAS (x-ray absorption spectroscopy), and NEXAFS (near edge x-ray fine structure) experiments, as well as with new experimental PES (photoemission experiments) data (III A) and recent ARPES experiments (subsections III B and III C). We conclude the paper with a summary. IV

II. ELECTRONIC STRUCTURE

A. LDA band structure

Sr_2RuO_4 has the undistorted single-layered K_2NiF_4 -type structure with the space group $I4/mmm$ and lattice parameters $a=b=3.8603 \text{ \AA}$, $c=12.729 \text{ \AA}$.⁴⁴ The structure is formed by layers of RuO_6 -octahedra separated by Sr-ions. The RuO_6 -octahedra are slightly elongated along the c -axis. Therefore the coordination of Ru-ions locally has a tetragonal symmetry.

Our first-principle calculation of the electronic structure of Sr_2RuO_4 is based on density functional theory (DFT) within the LDA approximation^{45,46} using the linearized muffin-tin orbitals (LMTO) method.⁴⁷ The partial densities of states for Sr_2RuO_4 are shown in Fig. 1. They are in good agreement with results of previous calculations.^{6,7,8,31,32} The strontium $4d$ states are almost empty and lie above 3 eV; the O- $2p$ derived bands are filled and extend from -8 eV to -1 eV.

Physically most interesting are the partially filled ruthenium $4d$ -states. Due to the octahedral coordination of the oxygen ions, the Ru- $4d$ states are split into t_{2g} and e_g orbitals (see Fig. 2). Owing to the stronger hybridization of the two e_g orbitals with oxygen p -states the corresponding bands lie above the three t_{2g} bands in the energy region from 0.5 eV to 5 eV. In Sr_2RuO_4 four Ru- $4d$ electrons occupy the three t_{2g} bands (d^4 configuration). The layered crystal structure of Sr_2RuO_4 results in a two-dimensional DOS of the xy orbital while the xz , yz orbitals have nearly one-dimensional character (see Fig. 2). The xy orbital hybridizes with xy orbitals of the four Ru neighbors and thus has a bandwidth almost twice as large ($W_{xy}=2.8 \text{ eV}$) as that of the xz , yz orbitals ($W_{xz,yz}=1.5 \text{ eV}$) which hybridize with corresponding orbitals of two Ru neighbors only.

The LDA bands in the energy window $-3 \dots 1 \text{ eV}$ are shown in Fig. 3. In contrast to a typical d^1 systems,²⁵ there is no well-pronounced separation of the oxygen $2p$ and ruthenium $4d$ states in Sr_2RuO_4 . More precisely, Fig. 3 shows that while the Ru- $4d$ xz , yz orbitals are separated from the oxygen $2p$ bands the Ru- $4d$ xy orbital strongly overlaps with these oxygen bands.

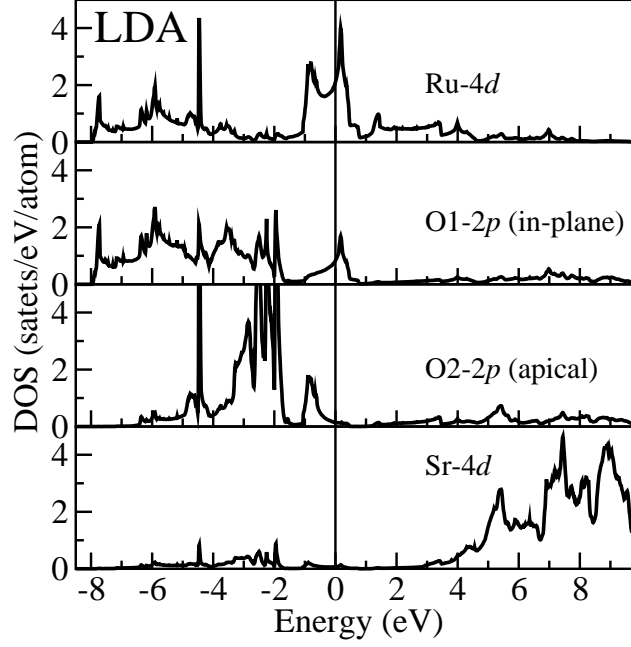


FIG. 1: Partial LDA DOS for Sr_2RuO_4 . The Fermi level corresponds to zero.

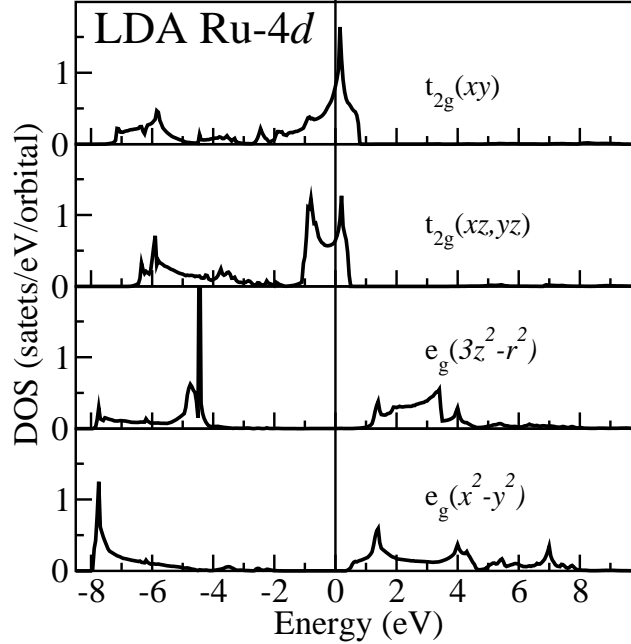


FIG. 2: Orbitaly projected LDA Ru-4d DOS. The Fermi level corresponds to zero.

B. LDA+DMFT(QMC) results: effect of correlations

Sr_2RuO_4 is a paramagnetic metal.¹ It is well known that the paramagnetic state of a correlated metal is well described by the DMFT (for reviews see^{48,49,50}). Within DMFT the electronic lattice problem is mapped onto a single-impurity Anderson model with a self-consistency condition.^{51,52} This mapping, which becomes exact in the limit of large coordination number of the lattice,⁵³ allows one to investigate the dynamics of correlated lattice electrons non-perturbatively at all interaction strengths. We use the LDA+DMFT *ab initio* technique^{17,18,19,23} (for an

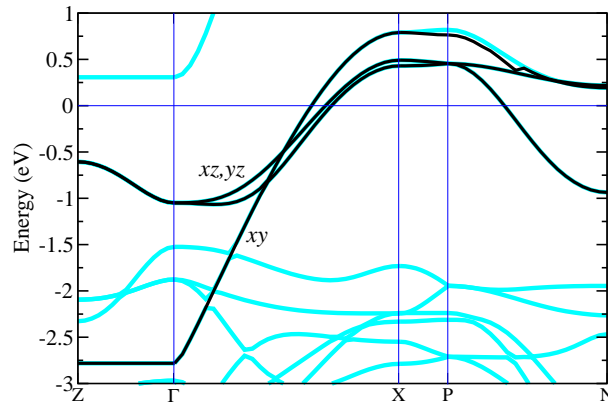


FIG. 3: (Colour online) Sr_2RuO_4 LDA band structure along high symmetry directions of the Brillouin zone. Light line - LDA bands, dark line - bands obtained by Wannier function projection on t_{2g} orbitals. The Fermi level corresponds to zero.

introduction see,²² for reviews see^{20,21,54,55}) to investigate correlation effects in Sr_2RuO_4 . The effective impurity problem corresponding to the many-body Hamiltonian is solved by quantum Monte Carlo simulations.⁵⁶ The LDA+DMFT approach was recently improved by employing a Wannier functions (WF) formalism,⁴³ which allows one to project the Hamilton matrix from the full-orbital space to a selected set of relevant orbitals. The projection ensures that the information about all states in the system is kept. In the present work we use the WF formalism to construct an effective few-orbital Hamiltonian with t_{2g} symmetry and to take into account the influence of correlated t_{2g} -orbitals on other states. A three-orbital Hamiltonian obtained by the WF projection with dispersions presented in Fig. 3 (black lines) was used as an *ab initio* setup of the correlation problem. *Ab initio* values of the orbitally averaged Coulomb interaction parameter $\bar{U}=1.7$ eV and Hund exchange parameter $J=0.7$ eV were obtained by constrained LDA calculations.⁵⁷ We emphasize that not only the on-site e_g screening and the screening from Ru-ions of the RuO_2 plane were taken into account in the calculation of the Coulomb interaction parameter but also screening from neighboring RuO_2 planes.

In the particular case of three t_{2g} -orbitals \bar{U} is equal to the inter-orbital Coulomb repulsion U' .^{17,18} Thus we obtain $U = U' + 2J = 3.1$ eV for the local intra-orbital Coulomb repulsion. We note that our values of U and J differ substantially from those by Liebsch and Lichtenstein⁴¹ who assumed a much smaller Hund exchange parameter. These authors estimated the Coulomb repulsion parameter from the XPS spectrum³⁴ using the position of the resonance satellite. The value of about 1.5 eV obtained thereby agrees well with our calculated value for \bar{U} .

The three-orbital, projected Hamiltonian together with the *ab initio* Coulomb interaction parameters were used as input for the QMC simulation of the effective quantum impurity problem arising in the DMFT. The simulations were performed for an inverse temperature $\beta=10$ eV⁻¹ using 40 imaginary time slices ($\Delta\tau=0.25$). The imaginary time QMC data were analytically continued by maximum entropy.⁵⁸ The results are shown in Fig. 4. We find a pronounced lower Hubbard band (LHB) between -5 and -1 eV, a quasiparticle peak (QP) around the Fermi level, and an upper Hubbard band (UHB) at about 1.5 eV. Real and imaginary parts of the corresponding self-energy for real frequencies (for details see Appendix B in⁴³) for t_{2g} orbitals are shown in Fig. 5. The mass enhancement calculated from the derivative of $\text{Re}\Sigma$ at the Fermi level amounts to 2.62 for the xy orbital and 2.28 for the xz, yz orbitals, in agreement with results from ARPES,⁴ dHvA³ and infrared optical experiments.⁵ A detailed analysis of the structures seen in Fig. 4 is presented in Appendix .

After having calculated the self-energy $\Sigma(\omega)$ for real frequencies one may perform the inverse transformation from the reduced Wannier basis back to the full LMTO basis.⁴³ This step allows one to take into account the influence of the three correlated t_{2g} orbitals on all other states of ruthenium, oxygen and strontium. The comparison of the noninteracting LDA partial density of states with the one obtained by the inverse transformation is shown in Fig. 6. Since the hybridization of Ru and O is quite strong the oxygen states are changed rather significantly by correlation effects on Ru-ions. These changes are most pronounced in the energy region between -4 and -1 eV. One can see that apical oxygen atoms are more affected by correlations than in-plane atoms. We believe that this is due to the one-dimensional character of the xz, yz states of the Ru-4d shell. Hence correlation effects are much stronger for these orbitals; consequently the DOS for the apical oxygen atoms is strongly modified. The strontium states are less affected.

A comparison between the partial LDA DOS of Ru-4d and the DOS obtained using the full-orbital self-energy from our LDA+DMFT(QMC) calculations is shown in Fig. 7. The main effect of the correlations on the Ru site is seen to be a transfer of spectral weight from the energy region near the Fermi level to the lower and upper Hubbard bands

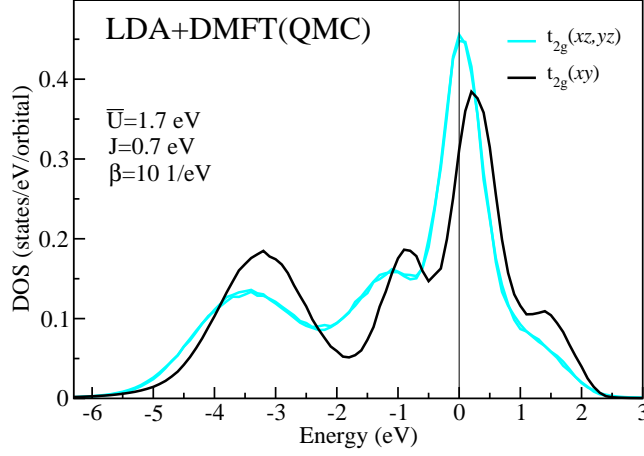


FIG. 4: (Colour online) Ru-4d(t_{2g}) spectral functions obtained within LDA+DMFT (QMC) using a projected Hamiltonian. Dark curve: xy orbital, light curve: xz, yz orbitals; $\bar{U}=1.7$ eV, $J=0.7$ eV. The Fermi level corresponds to zero.

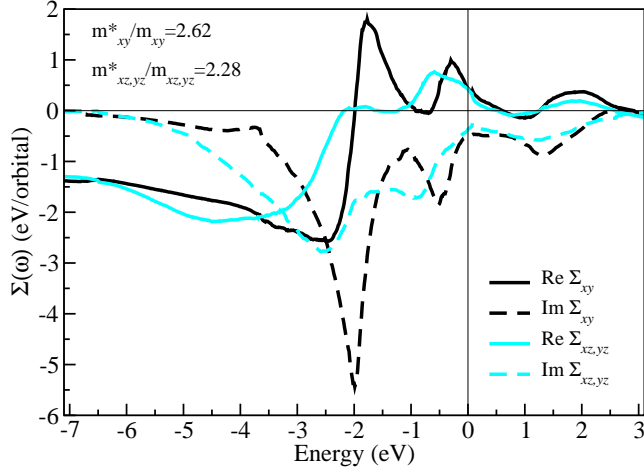


FIG. 5: (Colour online) Self-energy on the real energy axis for xy (black line) and xz, yz (light line) orbitals of Sr_2RuO_4 . Solid line: real part; dashed line: imaginary part. The Fermi level corresponds to zero.

range from -4 eV to -1 eV, and from 1 eV to 2 eV respectively.

III. COMPARISON WITH EXPERIMENTAL DATA

A. XPS and PES experiments

We will now compare the computed LDA+DMFT(QMC) spectral functions for the t_{2g} electrons (light solid lines in Fig. 8, 9, 10) and those calculated using the full-orbital self-energy (black solid lines in the same figures) with several experimentally obtained spectra describing both valence and conduction bands. To compare with experiment we took into account the photoemission cross section ratio for Ru-4d and O-2p states as a function of photon energy.⁵⁹ We found that, in general, an energy dependent broadening of the theoretical spectral functions gives better agreement with the experimental data (see⁶⁰ and⁶¹). For this the theory curves were convoluted using a Gaussian with a full width at half maximum increasing as $C \cdot E + g$. Here E is the binding energy, g is the experimental resolution, and C characterizes the increase of the broadening with energy upon moving away from Fermi level due to core-hole life time effects. The maximally allowed broadening was restricted to 1 eV. Specific values of C and g parameters used for comparison with experiment are indicated in the corresponding figures.

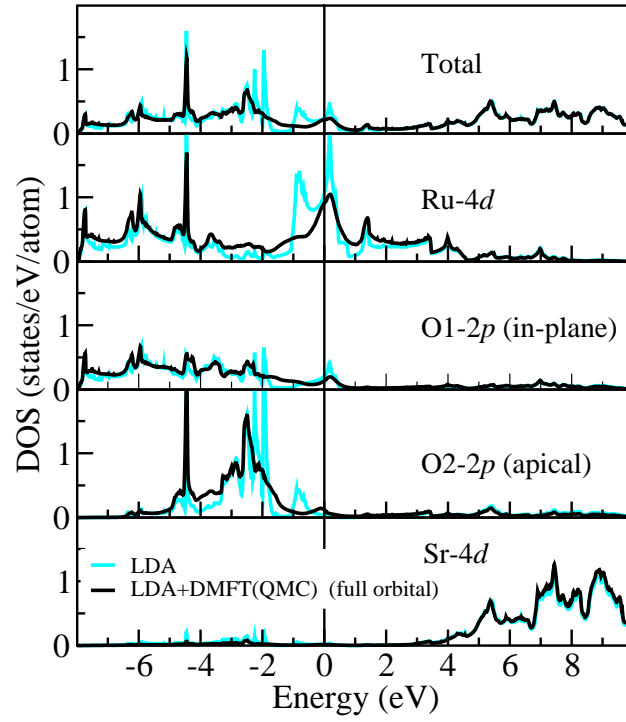


FIG. 6: (Colour online) Comparison of the total and partial LDA DOS (light curve) and the DOS calculated using the full-orbital self-energy from LDA+DMFT(QMC) (black curve). The Fermi level corresponds to zero.

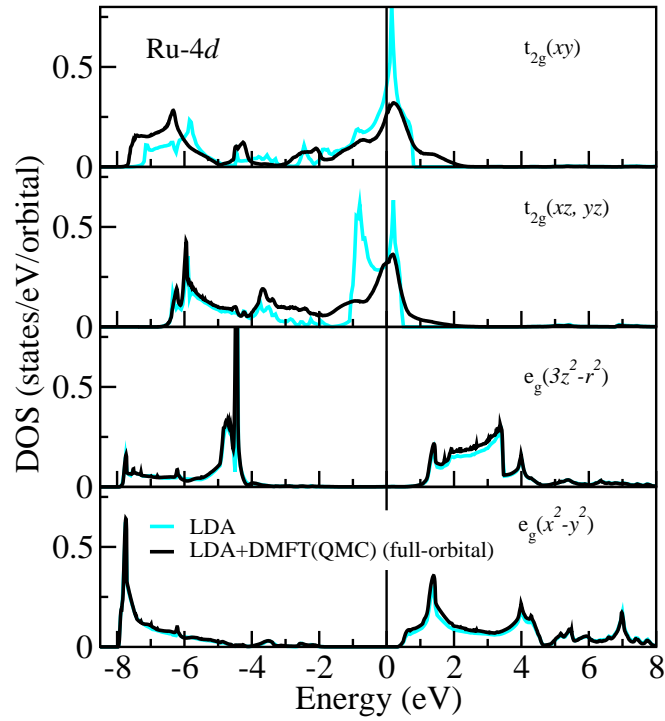


FIG. 7: (Colour online) The same as in Fig. 6 but for Ru-4d states only.

1. Comparison with previous XPS experiments

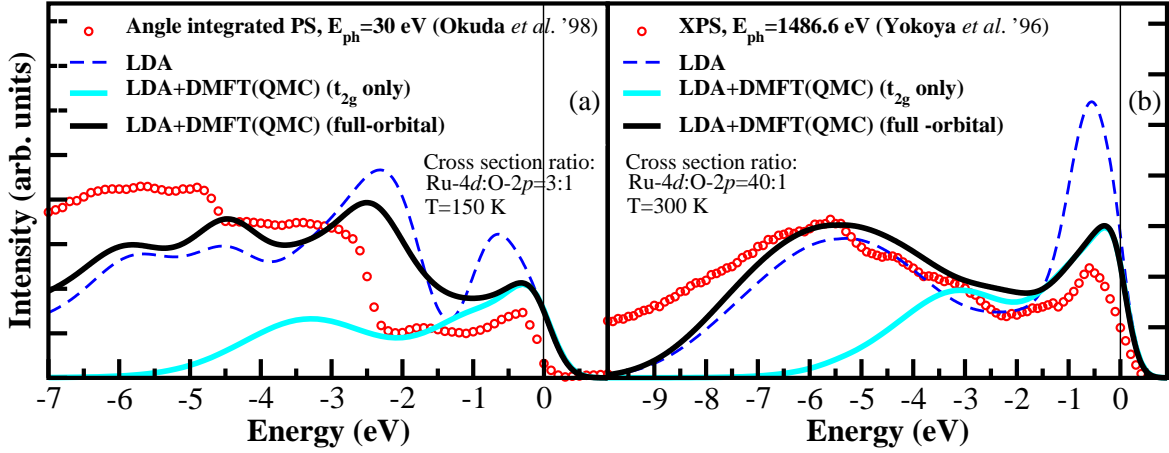


FIG. 8: (Colour online) Theoretical spectral functions of Sr_2RuO_4 calculated by LDA+DMFT(QMC); light solid line: t_{2g} orbitals, black solid line: full-orbital self-energy. In (a) the results are compared to an angle-integrated valence band photoemission spectrum¹¹ obtained with a photon energy $E_{\text{ph}} = 30$ eV, while in (b) we compare to an XPS spectrum obtained with a photon energy $E_{\text{ph}} = 1486.6$ eV.¹² The theoretical spectra are convoluted using a linear broadening $-0.04 \cdot E + 0.25$ for (a), and $-0.14 \cdot E + 0.25$ for (b) to account for the experimental resolution. Intensities are normalized on the area under curves. The Fermi level corresponds to zero.

In Fig. 8 we compare an angle integrated valence band photoemission spectrum of Sr_2RuO_4 ¹¹ [Fig. 8(a)] and the XPS spectra from Ref.¹² [Fig. 8(b)] with the theoretical spectral functions. The contributions from Ru-4d and O-2p spectra were weighted according to the photoemission cross section ratio⁵⁹ 3:1 for Fig. 8(a), corresponding to a photon energy 30 eV, and 40:1 for Fig. 8(b), corresponding to a photon energy of 1486.6 eV. The theoretical spectra were multiplied with the Fermi function at $T = 150$ K and 300 K, respectively. In Fig. 8 a linear broadening was employed. UPS (ultra-violet photoemission) data of the valence band of Sr_2RuO_4 ⁹ obtained at higher photon energy of 60 eV and 110 eV show similar features as the PES and XPS spectra in Fig. 8.

We note that for energies below -2 eV the weight of oxygen states in the spectrum (according to the cross section ratio) becomes essential. Indeed, only by proper inclusion of this contribution can a satisfactory description of the experimental spectra with the full-orbital LDA+DMFT(QMC) spectral function be achieved.

The experimental spectrum in Fig. 8(a) was obtained at a rather low photon energy. Therefore, according to the cross section ratio, the contribution of oxygen states is considerable. The calculated curves reproduce all features of the complicated structure of the experimental data, although the positions and weight of peaks agree only qualitatively. The most serious disagreement with experiment can be observed in the energy region from -2.5 eV up to the Fermi level. Despite similar line shapes the theoretical curves have too little weight. This failure can, for example, be attributed to an underestimation of the oxygen contribution in the theoretical curves, or to matrix element effects which may be significant at low photon energies. Nevertheless, the LDA+DMFT(QMC) spectra are seen to be in much better agreement with experiment than the LDA results. In particular, in LDA+DMFT the LDA peak near -0.5 eV is merely becomes a plateau – the redistribution of spectral weight obviously being an effect of correlations. Comparing the theoretical t_{2g} and full-orbital spectra with experiment, one can see that the latter yield a much better description in a wide energy range.

The XPS spectrum in Fig. 8(b) obtained at a very high photon energy is seen to be almost exclusively Ru-4d states. Obviously, the full-orbital spectral function gives good agreement with the XPS data. Moreover, one observes a pronounced maximum at -3 eV which experimentalists previously interpreted as the LHB.¹² This conjecture is now confirmed by our calculations (see the detailed discussion below).

2. Comparison with new PES experiment

Clean (001) surfaces of high purity single crystal samples were obtained by *in situ* cleavage at 20 K in ultrahigh vacuum. Angle-integrated and angle-resolved spectra were measured using the GAMMADATA-SCIENATA SES200 Analyzer at BL25SU of SPring-8 by use of circularly polarized light. Both measurements were performed at 700 eV by

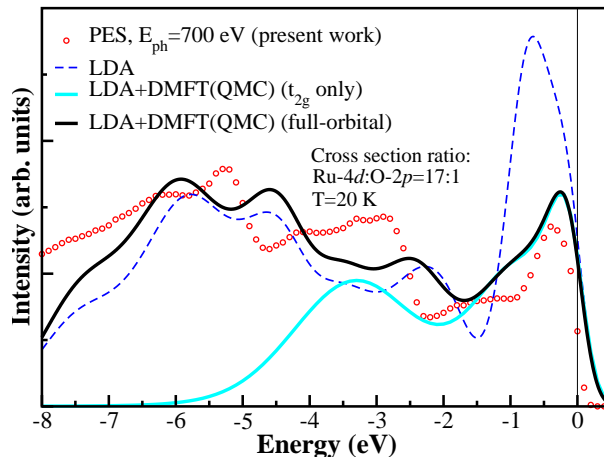


FIG. 9: (Colour online) Similar plot as in Fig. 8 but now we compare with PES spectrum of Sr_2RuO_4 . The theoretical spectra are convoluted using a linear broadening $-0.04 \cdot E + 0.20$ to account for the experimental resolution.

detecting near normal emission electrons to obtain highest bulk sensitivity at this photon energy. The resolution for these measurements was set to 200 meV (Fig. 9) and 120 meV (Fig. 11), respectively. The energy scale was calibrated by the Fermi edge of Au. The surface cleanliness was checked by the absence of possible additional spectral weight on the higher binding energy side of the O 1s peak, and by the absence of the C 1s contribution.

In Fig. 9 we compare photoemission spectrum of Sr_2RuO_4 with spectral functions calculated by LDA+DMFT(QMC). A weighted sum of Ru-4d and O-2p spectral functions according to the photoemission cross section ratio 17:1⁵⁹ was used – corresponding to an experimental photon energy of 700 eV. Theoretical spectra were multiplied with the Fermi function at 20 K and were linearly broadened to account for the experimental resolution.

3. Interpretation

We now discuss and interpret the experimental and theoretical spectra, and also check the presence of a LHB in the computed spectra. In Fig. 8(b) the structure in the experimental XPS-spectrum at -3 eV was interpreted as the LHB.¹² In the full-orbital LDA+DMFT(QMC) spectral function (black solid line) a corresponding feature is indeed visible, but has less intensity and appears only as a shallow shoulder rather than a distinct bulge. This structure is obviously not described by LDA (dashed line). Looking at the light solid line in Fig. 8(b) which represents the LDA+DMFT(QMC) DOS for the t_{2g} orbitals alone, we are able to identify this shoulder unambiguously as a result of the LHB. Thus we have theoretically confirmed the interpretation of Yokoya *et al.*¹² A very similar feature corresponding to the LHB in our LDA+DMFT(QMC) DOS was reported in Ref.¹⁵.

The situation is similar in the PES spectrum. Because of lower photon energies, and due to the enhancement of the O-2p contribution in the PES spectrum seen in Fig. 9, one again cannot identify the -3 eV satellite directly. However, one can recognize a feature in the spectrum whose position coincides with the LHB in our LDA+DMFT(QMC) calculations. In the first theoretical DMFT work on the ruthenate,⁴¹ model-Coulomb parameters were chosen as $\bar{U}=0.8$ eV and $J=0.2$ eV. As a consequence a less well-defined LHB with low spectral weight was obtained.

B. XAS and NEXAFS experiments

In Fig. 10(a) the O-1s x-ray absorption spectrum (XAS) of Sr_2RuO_4 ¹⁰ representing the conduction band is compared with the O-2p spectral function calculated via LDA+DMFT(QMC). Furthermore, Fig. 10(b) shows the near edge x-ray fine structure spectrum (NEXAFS) of Sr_2RuO_4 ⁹ together with the theoretical spectral functions. The theoretical spectra are multiplied with the Fermi function at $T = 300$ K and convoluted using linear broadening to account for the experimental resolution.

The agreement between theory and experiment in Fig. 10 is found to be only qualitative. This may be due to empty states (conduction band) in the LMTO method. Namely, the conventional LMTO choice of the MTO linearization energy point lies inside the occupied part of the bands. As a result the unoccupied states in LDA calculation are not

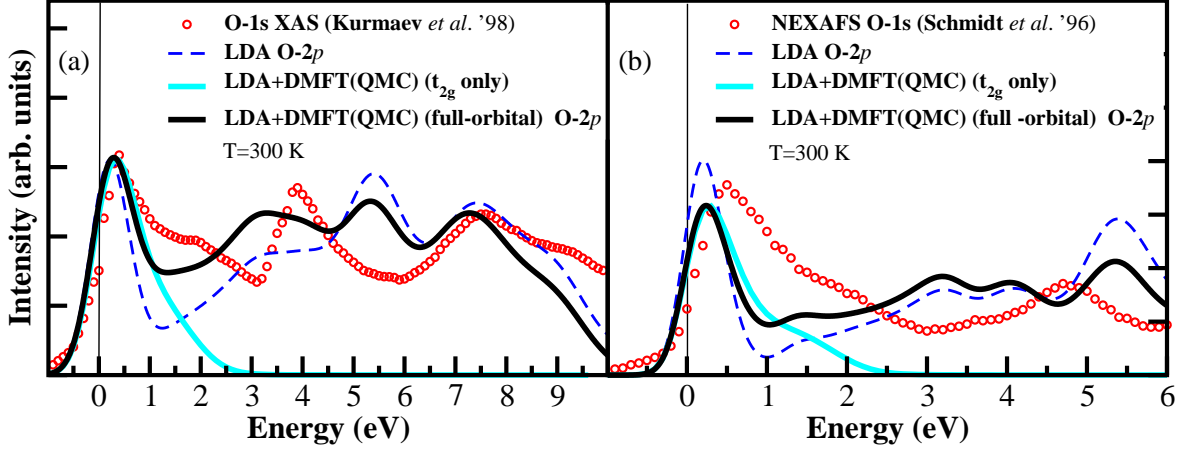


FIG. 10: (Colour online) Theoretical spectra of Sr_2RuO_4 calculated by LDA+DMFT(QMC); light solid line: only t_{2g} electrons, black solid line: full-orbital self-energy using O-2p states. (a) Comparison with O-1s XAS spectrum,¹⁰ (b) comparison with NEXAFS spectrum.⁹ Theoretical spectra are convoluted using linear broadening $0.01 \cdot E + 0.35$ for (a), and $0.02 \cdot E + 0.2$ for (b) to account for the experimental resolution. Intensities are normalized on the area under curves. The Fermi level corresponds to zero.

properly described. Nevertheless, due to the spectral weight redistribution in DMFT calculation, the agreement with experiment is improved (black solid line) in comparison with the bare LDA O-2p DOS (light dashed line).

C. High-energy bulk ARPES experiment

The comparison of experimental and theoretical spectra presented in the previous sections proves the existence of a LHB in Sr_2RuO_4 . Hence Sr_2RuO_4 must be considered a strongly correlated electron material. Further evidence for correlation effects comes from the renormalization of quasiparticle properties, i.e., effective masses and band dispersions. This renormalization was addressed by Liebsch and Lichtenstein⁴¹ who derived quasiparticle bands from self-consistent second-order self-energy. The Coulomb repulsion and Hund's rule exchange parameters chosen by these authors were rather small ($U=1.2\text{-}1.5$ eV, $J=0.2\text{-}0.4$ eV), resulting in a LHB with low spectral weight; nevertheless the effective masses ($m^* \approx 2.1 - 2.6$) were found to be in good agreement with experiments. In our investigation we determined the local Coulomb repulsion by the *ab initio* constrained LDA yielding $\bar{U}=1.7$ eV and $J=0.7$ eV, i.e., a value of $U=3.1$ eV which is twice as large as that used in Ref.⁴¹. This value of U now produces a pronounced LHB and, at the same time, gives almost the same values of m^*/m as those reported in Ref.⁴¹: $m^*/m=2.62$ for the xy orbital and 2.28 for the xz, yz orbitals, respectively. All these values are in good agreement with experimental estimations.^{3,4,5}

We will now proceed to calculate *k*-resolved spectra and quasiparticle band dispersions following the strategy proposed in Ref.^{41,62,63} and employed by us to calculate the ARPES spectra of SrVO_3 .⁶² ARPES computations have previously been performed also for the 2D Hubbard model by Maier *et al.*⁶⁴ in the framework of the dynamical cluster approximation (DCA),⁶⁵ and by Sadovskii *et al.*⁶⁶ within the so-called DMFT+ $\Sigma_{\mathbf{k}}$ approach.

To compare theoretical quasiparticle bands with the dispersion extracted from high-energy ARPES data we first calculate the *k*-resolved spectral function $A(\mathbf{k}, \omega)$ for Sr_2RuO_4 (for details see⁶²) defined by

$$A(\mathbf{k}, \omega) = -\frac{1}{\pi} \text{ImTr} \mathbf{G}(\mathbf{k}, \omega). \quad (1)$$

This quantity is determined by the diagonal elements of the Green function matrix in orbital space

$$\mathbf{G}(\mathbf{k}, \omega) = [\omega - \Sigma(\omega) - \mathbf{H}_0^{\text{WF}}(\mathbf{k})]^{-1}, \quad (2)$$

where \mathbf{H}^{WF} is the few-orbital Hamiltonian with t_{2g} symmetry obtained by WF projection. The corresponding eigenvalues are pictured in Fig. 3 as black lines. Since QMC only provides the self-energy Σ for Matsubara frequencies $i\omega_n$ and the *local* spectrum $A(\omega)$, the calculation of $A(\mathbf{k}, \omega)$ requires a method to compute Σ for real frequencies ω .

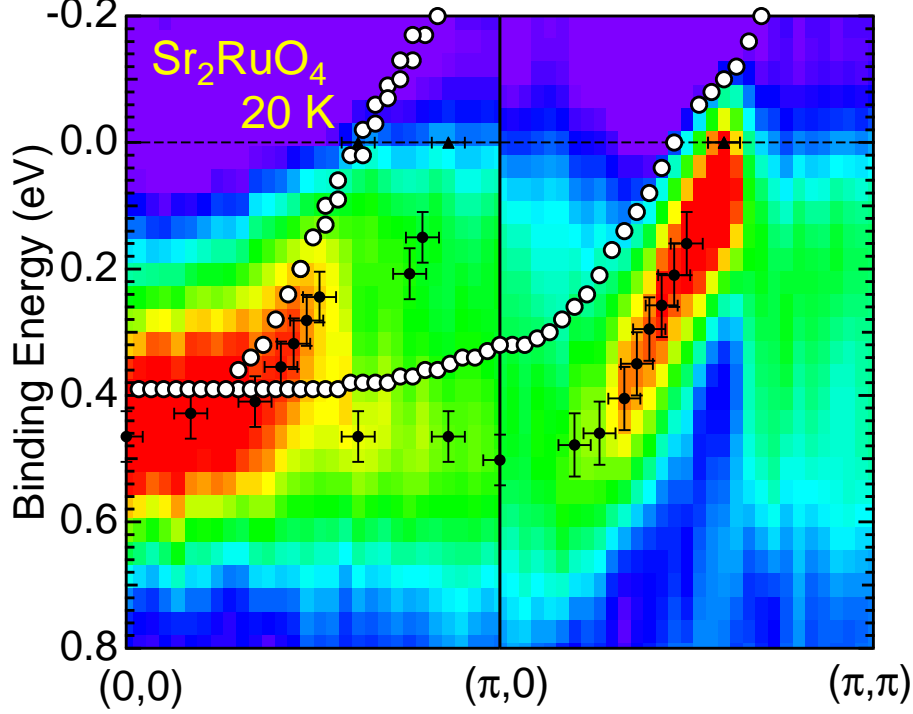


FIG. 11: (Colour online) Comparison of the dispersion extracted from high-energy ARPES data⁶⁷ and LDA+DMFT(QMC). Experimental data contain the second derivative of the energy distribution curves, peak positions of the second derivative (black dots), and k_F estimated from the momentum distribution curves at E_F (triangles). The theoretical dispersion is indicated by open circles.

This is achieved by first employing Kramers-Kronig to obtain

$$G(\omega + i\eta) = \int_{-\infty}^{\infty} d\omega' \frac{A(\omega')}{\omega - \omega' + i\eta}. \quad (3)$$

The local Green function and the complex self-energy are related by the \mathbf{k} -integrated Dyson equation

$$G(\omega) = \int_{\text{BZ}} d\mathbf{k} [\omega + \mu - \Sigma(\omega) - \mathbf{h}_0^{\text{eff}}(\mathbf{k})]^{-1}. \quad (4)$$

Solving Eq. (4) for given $G(\omega)$ for the self-energy $\Sigma(\omega)$ leads to the results presented in Fig. 5, which are then inserted into Eq. (2) to obtain the spectral function $A(\mathbf{k}, \omega)$ from Eq. (1). The maxima of $A(\vec{k}, \omega)$ obtained from this procedure are shown in Fig. 11 as black dots without error bars. Compared to experimental results our theoretical quasiparticle bands are shifted by -0.08 eV.

ARPES data directly provide the energy distribution curves,^{67,68} whose second derivative represents the dispersion, which is shown in Fig. 11 by a “rainbow scale”, red being the highest energy. Closed circles with error bars denote the peak positions of the second derivative. The Fermi momenta k_F estimated from the momentum distribution curves (MDCs)⁶⁷ at E_F are shown by triangles. We see that in the experiment there are two bands crossing the Fermi level at different \mathbf{k} -points in the $(0,0)$ - $(\pi,0)$ direction. There are also two bands in the calculated dispersion curve but they are almost degenerate. Nevertheless the position of the bottom of quasiparticle bands, the intersection with the Fermi level, and the shape of the experimental and theoretical dispersions qualitatively agree.

IV. CONCLUSION

In this paper we focused on the long-standing controversy concerning the strength of correlation effects in Sr_2RuO_4 , i.e., on the question whether Sr_2RuO_4 should be considered a strongly correlated electron material. This is generally the case if the ratio of Coulomb interaction and kinetic energy (bandwidth) is larger than unity. In particular, electronic correlations lead to a typical redistribution of spectral weight and thereby to the formation of well pronounced lower and upper Hubbard bands (LHB, UHB). We note that even on the experimental level the unambiguous identification of a maximum in the spectrum of Sr_2RuO_4 is made complicated by the overlap of the Ru-4*d* and O-2*p* bands.

To answer this question we first calculated the electronic structure of Sr_2RuO_4 within the conventional band theory using LDA. The correlations were then taken into account in the framework of the LDA+DMFT(QMC) scheme using *ab initio* values for the Coulomb and Hund exchange parameters. We found that the ratio of Coulomb interaction and bandwidth is indeed larger than unity in Sr_2RuO_4 , despite the rather extended 4*d*-states of Ru, leading to a distinctive redistribution of spectral weight and to the formation of a well-pronounced LHB. By comparing our theoretical spectra with XPS experiments we unambiguously identified this LHB with the structure observed at -3 eV. By contrast, the LDA DOS shows no distinctive feature at that energy.

To describe the experimental spectra in a wide energy range we employed a Wannier function formalism to transform the self-energy operator back to the full-orbital basis. The theoretical spectra obtained in that way agree very well with high-photon energy photoemission data; in particular, they reproduce the shoulder in the spectrum caused by the LHB. The basic features of the low photon energy UPS and intermediate energy PES spectra are also reproduced by the LDA+DMFT(QMC). Quasiparticle bands induced by correlations with mass renormalization of about 2.5 agree well with results from ARPES, dHvA and infrared optical experiments. The LDA+DMFT(QMC) derived quasiparticle bands are even in quantitative agreement with the dispersion extracted from ARPES data. Taken together these results provide clear evidence for strong electronic correlation effects in Sr_2RuO_4 . Hence, although Sr_2RuO_4 is a 4*d* system it must be regarded as a strongly correlated electron material.

V. ACKNOWLEDGMENT

We thank R. Claessen, E.Z. Kurmaev, and A. Lichtenstein for helpful discussions. This work was supported by Russian Basic Research Foundation grants RFFI-GFEN-03-02-39024, RFFI-04-02-16096, RFFI-05-02-17244, RFFI-05-02-16301, by the Deutsche Forschungsgemeinschaft through Sonderforschungsbereiche 484 and 602, and in part by programs of the Presidium of the Russian Academy of Sciences (RAS) “Quantum macrophysics” and the Division of Physical Sciences of the RAS “Strongly correlated electrons in semiconductors, metals, superconductors and magnetic materials”. IN and ZP acknowledge support by the Russian Science Support Foundation, Dynasty Foundation and International Center for Fundamental Physics in Moscow. IN also appreciates the support from the Grant of President of Russian Federation for young scientists MK-2118.2005.02.

APPENDIX: ANALYSIS OF LDA+DMFT(QMC) SPECTRUM

An important first step in interpreting the structures in the DOS in Fig. 4 is to identify purely atomic excitations. These will of course be shifted and broadened by correlation effects, but should nevertheless still be prominent. These excitations can readily be obtained from the atomic level picture. We denote the bare level energy of the *xz*, *yz* orbitals as $\epsilon_{xz,yz} \equiv \epsilon_0$. Note that we do not know this value *a priori*, since it is neither the center-of-gravity of the bare LDA-DOS nor a particular peak position in the correlated DOS. It is, in fact, the unknown shift due to the double-counting correction of the LDA.

Hund exchange and Coulomb parameters from constrained LDA are $J = 0.7$ eV and $\bar{U} = 1.7$ eV. For three t_{2g} -orbitals we have $U' = \bar{U} = 1.7$ eV and thus $U = U' + 2J = 3.1$ eV. Finally, the splitting of the centers of gravity of the *xy* and *xz*, *yz* DOS is $\Delta\epsilon = \epsilon_{xy} - \epsilon_{xz,yz} = 0.1$ eV.

With these information we can construct the basis spanning the ground state and then calculate the excited states and their relative energies. Concentrating on a particular basis vector of the ground state manifold, we obtain the scheme in Tab. I, where we show the states contributing to the possible single-particle excitations. The corresponding excitation energies with the unknown level shift ϵ_0 are listed in the third column. Obviously, the transition $c_{xy}^\dagger|GS\rangle$ represents the excitation with the lowest energy of the *xy*-DOS, i.e., should be identified with the position of lowest peak at energy $E_1 = -3.2$ eV in the LDA+DMFT(QMC) DOS in Fig. 4, leading to $\epsilon_0 = -7$ eV and the final numerical values in the last column of Tab. I.

The identification of the further structures is now straightforward. For the *xy* orbital, we must attribute the peak around $E = 0.5$ eV to the excited states $c_{xy}^\dagger|GS\rangle$. Likewise, in the *xz*, *yz* manifold the peak at $E \approx -3.5$ eV

TABLE I: Ground-state as well as single-particle excitations and their energies.

	$ xz\rangle$	$ yz\rangle$	$ xy\rangle$	Energy E_α	Excitation energy ϵ	value, eV
Gs	$ \uparrow\downarrow\rangle$	$ \uparrow\rangle$	$ \uparrow\rangle$	$4\epsilon_0 + \Delta\epsilon + 6U - 13J$		
				occupied states $\epsilon = E_{\text{GS}} - E_\alpha$		
c_{xy}^\uparrow	$ \uparrow\downarrow\rangle$	$ \uparrow\rangle$	$ 0\rangle$	$3\epsilon_0 + 3U - 5J$	$\epsilon_0 + \Delta\epsilon + 3U - 8J = \epsilon_0 + 3.8$	-3.2
c_{xz}^\uparrow	$ \downarrow\rangle$	$ \uparrow\rangle$	$ \uparrow\rangle$	$3\epsilon_0 + \Delta\epsilon + 3U - 7J$	$\epsilon_0 + 3U - 6J = \epsilon_0 + 5.1$	-1.9
c_{yz}^\uparrow	$ \uparrow\downarrow\rangle$	$ 0\rangle$	$ \uparrow\rangle$	$3\epsilon_0 + \Delta\epsilon + 3U - 5J$	$\epsilon_0 + 3U - 8J = \epsilon_0 + 3.7$	-3.3
c_{xz}^\downarrow	$ \uparrow\rangle$	$ \uparrow\rangle$	$ \uparrow\rangle$	$3\epsilon_0 + \Delta\epsilon + 3U - 9J$	$\epsilon_0 + 3U - 4J = \epsilon_0 + 6.5$	-0.5
				empty states $\epsilon = E_\alpha - E_{\text{GS}}$		
c_{xy}^\dagger	$ \uparrow\downarrow\rangle$	$ \uparrow\rangle$	$ \uparrow\downarrow\rangle$	$5\epsilon_0 + 2\Delta\epsilon + 10U - 20J$	$\epsilon_0 + \Delta\epsilon + 4U - 7J = \epsilon_0 + 7.5$	0.5
c_{yz}^\dagger	$ \uparrow\downarrow\rangle$	$ \uparrow\downarrow\rangle$	$ \uparrow\rangle$	$5\epsilon_0 + \Delta\epsilon + 10U - 20J$	$\epsilon_0 + 4U - 7J = \epsilon_0 + 7.4$	0.4

corresponds to $c_{yz}^\uparrow|GS\rangle$, and the broad structure at $E \approx -1.3$ eV to a superposition of $c_{xz}^\uparrow|GS\rangle$ and $c_{xz}^\downarrow|GS\rangle$. The peak at $E \approx 0$ eV finally can be identified with $c_{xy}^\dagger|GS\rangle$.

Note that the peak in the xy -DOS at $E \approx -0.8$ eV has no correspondence in the atomic scheme. It could, however, be due to a finite admixture of the state $|\uparrow\rangle|\uparrow\rangle|\uparrow\downarrow\rangle$ to the ground-state of the interacting system. This state would then allow for an excitation involving c_{xy}^\dagger with an excitation energy -0.6 eV.

* Electronic address: pzv@optics.imp.uran.ru

- ¹ Y. Maeno, H. Hashimoto, K. Yoshida, S. Nishizaki, T. Fujita, J.G. Bednorz, and F. Lichtenberg, *Nature (London)* **372**, 532 (1994).
- ² M. Imada, A. Fujimori, and Y. Tokura, *Rev. Mod. Phys.* **70**, 1039-1263 (1998)
- ³ A. P. Mackenzie, S. R. Julian, A. J. Diver, G. J. McMullan, M. P. Ray, G. G. Lonzarich, Y. Maeno, S. Nishizaki, and T. Fujita, *Phys. Rev. Lett.* **76**, 3786 (1996); **78**, 2271 (1997).
- ⁴ A. V. Puchkov, Z.-X. Shen, T. Kimura, and Y. Tokura, *Phys. Rev. B* **58**, R13322 (1998).
- ⁵ T. Katsufuji, M. Kasai, and Y. Tokura, *Phys. Rev. Lett.* **76**, 126 (1996).
- ⁶ T. Oguchi, *Phys. Rev. B* **51**, 1385 (1995).
- ⁷ D. J. Singh, *Phys. Rev. B* **52**, 1358 (1995).
- ⁸ I. Hase and Y. Nishihara, *J. Phys. Soc. Jpn.* **65**, 3957 (1996).
- ⁹ M. Schmidt, T. R. Cummins, M. Bürk, D. H. Lu, N. Nücker, and S. Schuppler, F. Lichtenberg, *Phys. Rev. B* **53**, R14761 (1996).
- ¹⁰ E. Z. Kurmaev, S. Stadler, D. L. Ederer, Y. Harada, S. Shin, M. M. Grush, T. A. Callcott, R. C. C. Perera, D. A. Zatsopin, N. Ovechkina, M. Kasai, Y. Tokura, T. Takahashi, K. Chandrasekaran, R. Vijayaraghavan, and U. V. Varadaraju, *Phys. Rev. B* **57**, 1558 (1998).
- ¹¹ T. Okuda, H. Daimon, M. Kotsugi, K. Nakatsuji, M. Fujikawa, S. Suga, Y. Tezuka, S. Shin, M. Kasai, Y. Tokura, *J. Electron Spectrosc. Relat. Phenom.* **88-91**, 473 (1998).
- ¹² T. Yokoya, A. Chainani, T. Takahashi, and H. Katayama-Yoshida, M. Kasai, Y. Tokura, N. Shanthi and D. D. Sarma, *Phys. Rev. B* **53**, 8151 (1996).
- ¹³ I. H. Inoue, Y. Aiura, Y. Nishihara, Y. Haruyama, S. Nishizaki, Y. Maeno, T. Fujita, J. G. Bednorz, F. Lichtenberg, *Physica B* **223-224**, 516 (1996); I. H. Inoue, Y. Aiura, Y. Nishihara, Y. Haruyama, S. Nishizaki, Y. Maeno, T. Fujita, F. Lichtenberg, J. G. Bednorz, *J. Electron Spectrosc. Relat. Phenom.* **78**, 175 (1996).
- ¹⁴ I. H. Inoue, A. Kimura, A. Harasawa, A. Kakizaki, Y. Aiura, S. Ikeda, Y. Maeno, *J. Phys. Chem. Solids* **59**, No. 10-12, 2205 (1998).
- ¹⁵ T. T. Tran, T. Mizokawa, S. Nakatsuji, H. Fukazawa, and Y. Maeno, *Phys. Rev. B* **70**, 153106 (2004).
- ¹⁶ A. Fujimori, I. Hase, H. Namatame, Y. Fujishima, Y. Tokura, H. Eisaki, S. Uchida, K. Takegahara, F. M. F. de Groot, *Phys. Rev. Lett.* **69**, 1796 (1992).
- ¹⁷ V. I. Anisimov, A. I. Poteryaev, M. A. Korotin, A. O. Anokhin, and G. Kotliar, *J. Phys. Cond. Matter* **9**, 7359 (1997).
- ¹⁸ A. I. Lichtenstein, M. I. Katsnelson, *Phys. Rev. B* **57**, 6884 (1998).
- ¹⁹ I. A. Nekrasov, K. Held, N. Blümer, A. I. Poteryaev, V. I. Anisimov, and D. Vollhardt, *Euro. Phys. J. B* **18**, 55 (2000).
- ²⁰ K. Held, I. A. Nekrasov, G. Keller, V. Eyert, N. Blumer, A. K. McMahan, R. T. Scalettar, Th. Pruschke, V. I. Anisimov, and D. Vollhardt, *Psi-k Newsletter* **56**, 65 (2003) [psi-k.dl.ac.uk/newsletters/News_56/Highlight_56.pdf].

- ²¹ K. Held, I. A. Nekrasov, N. Blümer, V. I. Anisimov, and D. Vollhardt, *Int. J. Mod. Phys. B* **15**, 2611 (2001); K. Held, I. A. Nekrasov, G. Keller, V. Eyert, N. Blümer, A. K. McMahan, R. T. Scalettar, T. Pruschke, V. I. Anisimov, and D. Vollhardt, available as cond-mat/0112079 (Published in *Quantum Simulations of Complex Many-Body Systems: From Theory to Algorithms*, eds. J. Grotendorst, D. Marks, and A. Muramatsu, NIC Series Volume 10 (NIC Directors, Forschungszentrum Jülich, 2002) p. 175-209 (ISBN 3-00-009057-6); A. I. Lichtenstein, M. I. Katsnelson, G. Kotliar, in *Electron Correlations and Materials Properties 2nd ed.*, edited by A. Gonis, Nicholas Kioussis and Mikael Ciftan, Kluwer Academic/Plenum, p. 428, New York (2002), available as cond-mat/0112079.
- ²² G. Kotliar and D. Vollhardt, *Phys. Today* **57**, No. 3 (March), 53 (2004).
- ²³ M. B. Zöfl, Th. Pruschke, J. Keller, A. I. Poteryaev, I. A. Nekrasov, and V. I. Anisimov, *Phys. Rev. B* **61**, 12810 (2000).
- ²⁴ E. Pavarini, S. Biermann, A. Poteryaev, A. I. Lichtenstein, A. Georges, and O. K. Andersen, *Phys. Rev. Lett.* **92**, 176403 (2004).
- ²⁵ A. Sekiyama, H. Fujiwara, S. Imada, S. Suga, H. Eisaki, S. I. Uchida, K. Takegahara, H. Harima, Y. Saitoh, I. A. Nekrasov, G. Keller, D. E. Kondakov, A. V. Kozhevnikov, Th. Pruschke, K. Held, D. Vollhardt, and V. I. Anisimov, *Phys. Rev. Lett.* **93**, 156402 (2004).
- ²⁶ T. M. Rice and M. Sigrist, *J. Phys. Condens. Matter* **7**, L643 (1995).
- ²⁷ G. Baskaran, *Physica B* **224**, 490 (1996).
- ²⁸ A. P. Mackenzie, Y. Maeno, *Rev. Mod. Phys.* **75**, 657 (2003)
- ²⁹ C. Bergemann, A. P. Mackenzie, S. R. Julian, D. Forsythe, E. Ohmichi, *Adv. Phys.* **52**, No. 7, 639 (2003).
- ³⁰ I. I. Mazin and D. J. Singh, *Phys. Rev. Lett.* **79**, 733 (1997).
- ³¹ P. K. de Boer and R. A. de Groot, *Phys. Rev. B* **59**, 9894 (1999).
- ³² G. J. McMullan, M. P. Ray and R. J. Needs, *Physica B* **223-224**, 529 (1996).
- ³³ D. H. Lu, M. Schmidt, T. R. Cummins, and S. Schuppler, *Phys. Rev. Lett.* **76**, 4845 (1996)
- ³⁴ T. Yokoya, A. Chainani, T. Takahashi, H. Katayama-Yoshida, M. Kasai, and Y. Tokura, *Phys. Rev. Lett.* **76**, 3009 (1996).
- ³⁵ T. Yokoya, A. Chainani, T. Takahashi, H. Ding, J. C. Campuzano, H. Katayama-Yoshida, M. Kasai, Y. Tokura, *Phys. Rev. B* **54**, 13311 (1996).
- ³⁶ R. Matzdorf, Z. Fang, Ismail, Jiandi Zhang, T. Kimura, Y. Tokura, K. Terakura, E. W. Plummer, *Science* **289**, 746 (2000).
- ³⁷ A. Damascelli, D. H. Lu, K. M. Shen, N. P. Armitage, F. Ronning, D. L. Feng, C. Kim, Z.-X. Shen, T. Kimura, Y. Tokura, Z. Q. Mao, Y. Maeno, *Phys. Rev. Lett.* **85**, 5194 (2000).
- ³⁸ A. Damascelli, *Phys. Scripta* **109**, 61 (2004).
- ³⁹ A. Pérez-Navarro, J. Costa-Quintana, and F. López-Aguilar, *Phys. Rev. B* **61**, 10125 (2000).
- ⁴⁰ R. Arita, S. Onari, K. Kuroki, H. Aoki, *Physica B* **359-361** 584 (2005).
- ⁴¹ A. Liebsch and A. Lichtenstein, *Phys. Rev. Lett.* **84**, 1591 (2000).
- ⁴² V. I. Anisimov, I. A. Nekrasov, D. E. Kondakov, T. M. Rice, and M. Sigrist, *Eur. Phys. J. B* **25**, 191 (2002).
- ⁴³ V. I. Anisimov, D. E. Kondakov, A. V. Kozhevnikov, I. A. Nekrasov, Z. V. Pchelkina, J. W. Allen, S.-K. Mo, H.-D. Kim, P. Metcalf, S. Suga, A. Sekiyama, G. Keller, I. Leonov, X. Ren, and D. Vollhardt, *Phys. Rev. B* **71**, 125119 (2005).
- ⁴⁴ M. Braden, A. H. Moudden, S. Nishizaki, Y. Maeno and T. Fujita, *Physica C* **273**, 248 (1997).
- ⁴⁵ W. Kohn and L. J. Sham, *Phys. Rev.* **140**, A1133 (1965); L. J. Sham and W. Kohn, *Phys. Rev.* **145**, 561 (1966).
- ⁴⁶ L. Hedin and B. I. Lundqvist, *J. Phys. C* **4**, 2064 (1971); U. von Barth and L. Hedin, *ibid.* **5**, 1629 (1972).
- ⁴⁷ O. K. Andersen, *Phys. Rev. B* **12**, 3060 (1975); O. Gunnarsson, O. Jepsen, and O. K. Andersen, *Phys. Rev. B* **27**, 7144 (1983).
- ⁴⁸ D. Vollhardt, in *Correlated Electron Systems*, edited by V. J. Emery, World Scientific, Singapore, 1993, p. 57.
- ⁴⁹ Th. Pruschke, M. Jarrell, and J. K. Freericks, *Adv. Phys.* **44**, 187 (1995).
- ⁵⁰ A. Georges, G. Kotliar, W. Krauth, and M. J. Rozenberg, *Rev. Mod. Phys.* **68**, 13 (1996).
- ⁵¹ A. Georges and G. Kotliar, *Phys. Rev. B* **45**, 6479 (1992).
- ⁵² M. Jarrell, *Phys. Rev. Lett.* **69**, 168 (1992).
- ⁵³ W. Metzner and D. Vollhardt, *Phys. Rev. Lett.* **62**, 324 (1989).
- ⁵⁴ G. Kotliar, S.Y. Savrasov, K. Haule, V.S. Oudovenko, O. Parcollet, C.A. Marianetti, preprint cond-mat/0511085 (submitted to Review of Modern Physics).
- ⁵⁵ K. Held, Preprint cond-mat/0511293.
- ⁵⁶ J. E. Hirsch and R. M. Fye, *Phys. Rev. Lett.* **56**, 2521 (1986); M. Jarrell, *Phys. Rev. Lett.* **69**, 168 (1992); M. Rozenberg, X. Y. Zhang, and G. Kotliar, *Phys. Rev. Lett.* **69**, 1236 (1992); A. Georges and W. Krauth, *Phys. Rev. Lett.* **69**, 1240 (1992); M. Jarrell in *Numerical Methods for lattice Quantum Many-Body Problems*, edited by D. Scalapino, Addison Wesley, 1997.
- ⁵⁷ O. Gunnarsson, O. K. Andersen, O. Jepsen, and J. Zaanen, *Phys. Rev. B* **39**, 1708 (1989); V. I. Anisimov and O. Gunnarsson *ibid.* **43**, 7570 (1991).
- ⁵⁸ For a review on the maximum entropy method see Mark Jarrell and J. E. Gubernatis, *Phys. Rep.* **269**, 133 (1996).
- ⁵⁹ J. J. Yeh, I. Lindau, *Atomic Data and Nuclear Data Tables* (Academic, New York, 1985), Vol. 32(1).
- ⁶⁰ L. Z. Liu, J. W. Allen, O. Gunnarsson, N. E. Christensen, O. K. Andersen, *Phys. Rev. B* **45**, 8934 (1992).
- ⁶¹ A. J. Arko, J. J. Joyce, L. Morales, J. Wills, J. Lashley, F. Wastin, J. Rebizant, *Phys. Rev. B* **62**, 1773 (2000).
- ⁶² I. A. Nekrasov, K. Held, G. Keller, D. E. Kondakov, Th. Pruschke, M. Kollar, O. K. Andersen, V. I. Anisimov, D. Vollhardt, cond-mat/0508313.
- ⁶³ S. Biermann, A. Dallmeyer, C. Carbone, W. Eberhardt, C. Pampuch, O. Rader, M. I. Katsnelson, and A. I. Lichtenstein, *JETP Letters* **80**, 612 (2005).
- ⁶⁴ Th. A. Maier, Th. Pruschke, and M. Jarrell, *Phys. Rev. B* **66**, 075102 (2002).
- ⁶⁵ C. Huscroft, M. Jarrell, Th. Maier, S. Moukouri, A. N. Tahvildarzadeh, *Phys. Rev. Lett.* **86**, 139 (2001); M.H. Hettler, M.

- Mukherjee, M. Jarrell, H.R. Krishnamurthy, Phys. Rev. B **61**, 12739 (2000); T. Maier, M. Jarrell, T. Pruschke, J. Keller, Eur. Phys. J. B **13**, 613 (2000); M. H. Hettler, A. N. Tahvildar-Zadeh, M. Jarrell, T. Pruschke, H. R. Krishnamurthy, Phys. Rev. B **58**, R7475 (1998); Th. Maier, M. Jarrell, Th. Pruschke, M. H. Hettler, Rev. Mod. Phys. **77**, 1027-1080 (2005).
- ⁶⁶ M. V. Sadovskii, I. A. Nekrasov, E. Z. Kuchinskii, Th. Pruschke, V. I. Anisimov, Phys. Rev. B **72**, 155105 (2005); E. Z. Kuchinskii, I. A. Nekrasov, and M. V. Sadovskii, JETP Letters **82**, 198 (2005).
- ⁶⁷ A. Sekiyama, S. Kasai, M. Tsunekawa, Y. Ishida, M. Sing, A. Irizawa, A. Yamasaki, S. Imada, T. Muro, Y. Saitoh, Y. Onuki, T. Kimura, Y. Tokura, and S. Suga, Phys. Rev. B **70**, 060506(R) (2004).
- ⁶⁸ A. Sekiyama and S. Suga, J. Electron Spectrosc. Relat. Phenom. **137-140**, 681-685 (2004).